Channel- and Angle-Resolved Above Threshold Ionization in the Molecular Frame

Jochen Mikosch,* Andrey E. Boguslavskiy, Iain Wilkinson, Michael Spanner,† Serguei Patchkovskii, and Albert Stolow‡

National Research Council of Canada, 100 Sussex Drive, Ottawa, Ontario K1A 0R6, Canada

(Received 10 September 2012; published 11 January 2013)

In strong-field ionization (SFI) of polyatomic molecules, the participation of multiple electronic ionization channels is emerging as a key aspect. In the molecular frame, each channel is expected to show a characteristic dependence of the SFI yield on the polarization direction of the ionizing field. We apply a new angle- and channel-resolved SFI technique to the polyatomic molecule 1,3-butadiene and compare these molecular-frame measurements with two leading theoretical models.

DOI: 10.1103/PhysRevLett.110.023004 PACS numbers: 33.80.Rv, 33.60.+q, 42.50.Hz

Intense laser fields can exert electric forces on valence electrons exceeding those that bind them to atoms and molecules, leading to ionization within a fraction of an optical cycle. This process lies at the heart of the burgeoning field of attosecond science [1]. Strong-field ionization (SFI) leads to phenomena such as above threshold ionization [2], high harmonic generation [3], and laser induced electron diffraction [4,5]. Adiabatic single active electron models of atomic SFI [6–8] do not translate well to the multielectron world of polyatomic molecules [9,10], inspiring extensions such as adiabatic molecular tunnelling theory [11] and molecular symmetry-based strong-field approximations [12]. The population of multiple ionic continua, often underestimated by atomiclike theories [13–16], is a key aspect of SFI in polyatomic molecules. More rigorous treatments of molecular SFI that incorporate electronic structure and multielectron effects include time-dependent density functional [17–19] and resolution-in-ionic-states [20] theories. Here, we present a channel- and angle-resolved study of molecular-frame (MF) SFI in a polyatomic molecule, the results of which provide stringent tests for theory.

SFI yields depend on the relative orientation of the molecular frame and the laser polarization direction [21–23]. This angular dependence reflects the nodal symmetries of the ionizing orbitals [12,24], as well as electron correlations [25,26], permanent dipole moments [27], and the short-range binding potential of the cation [20]. Consequently, each ionization channel should display a unique angular dependence of the SFI yields. Therefore, channel-integrated but angle-dependent studies will not be sufficient. We recently introduced the channel-resolved above threshold ionization (CRATI) method [16]. For molecules with dissociative excited ionic states, it directly resolves SFI into continuum channels correlating with the population of electronic ground (D_0) and/or excited (D_1, D_2, etc.) states of the cation. The method relies on covariant measurement of photoelectron and mass spectra averaged over a random molecular alignment distribution. Here, we combine the CRATI technique with laser alignment in order to determine the channel-resolved angular ionization probability in the molecular frame (MF-CAIP). We present MF-CAIP studies of D_0 and D_1 SFI in 1,3-butadiene (C_4H_6) and compare with the expectations of two theoretical models.

Fragment recoil momentum vector imaging can yield recoil-frame SFI angular distributions, as demonstrated for HCl [15], N_2, O_2, CO, CO_2, and C_2H_2 [21,28]. Transformation from the recoil frame to the MF requires the axial recoil approximation, which is questionable for polyatomic molecules. A more general approach is to align or orient molecules [29] before SFI: With this method, angle- but not channel-resolved AIPs were recorded. One-dimensional (1D) AIPs were obtained by scanning the SFI laser polarization with respect to the fixed-in-space molecular axis [22,30]. Full 3D orientation-dependent MF AIPs were achieved by utilizing circularly polarized light and recording the photoelectron angular istributions from the 3D oriented molecules [23,31,32].

SFI of 1,3-butadiene proceeds via both D_0 (90%) and D_1 (10%) channels at an intensity of 1.9×10^{13} W/cm^2 [16]. D_0 ionization yields the stable $C_4H_6^+$ parent ion, whereas D_1 ionization correlates with the formation of $C_3H_3^+$ and $C_4H_5^+$ fragments (see Fig. 1 of Ref. [16]). This correlation with a given channel permits measurement of the θ (polar angle) dependent, ϕ (azimuthal angle) averaged AIPs $S(\theta)$ independently for the D_0 and D_1 channels. The angle θ is defined with respect to the axis of maximum polarizability, which is offset by 8.5° from the principal axis with the lowest moment of inertia. We use unprimed (primed) variables to indicate molecular (lab) frame angles. In order to extract $S(\theta)$, we utilize 1D nonadiabatic molecular alignment. The peak alignment for 1,3-butadiene is achieved near the rotational half-revival, at time t_a following an alignment laser pulse. At this time delay, we measured $M(\alpha', t_a)$, the ionization yield as a function of the lab-frame angle α' between the polarization axes of the linearly polarized alignment and SFI lasers. $M(\alpha', t)$ is the convolution of $S(\theta)$ with the time-dependent 1D alignment distribution $A(\theta', \phi', t)$ [22],

$$M(\alpha', t) = \frac{1}{4\pi} \int_0^{2\pi} d\phi' \int_0^{\pi} d\theta' S[\theta(\theta', \phi'; \alpha')] \times A(\theta', \phi', t) \sin(\theta'), \quad (1)$$

where

$$\cos\theta = \cos\alpha' \cos\theta' - \sin\alpha' \sin\theta' \sin\phi'.$$

The 1D alignment distribution is cylindrically symmetric about the alignment laser polarization, also the main axis of the alignment distribution. Therefore, we can replace $A(\theta', \phi', t)$ in Eq. (1) by the ϕ'-averaged distribution $A(\theta', t)/2\pi$. A pulsed supersonic expansion of helium (40 bar) seeded with 0.01% 1,3-butadiene was intersected by the focus of an alignment laser [$\lambda_p = 2100$ nm, 120 μm focal spot size, 285(30) fs FWHM pulse length, intensity 4×10^{12} W/cm^2] and a time-delayed SFI laser [$\lambda_e = 795.5$ nm, 40 μm, 40(5) fs] in the interaction region of a magnetic bottle photoelectron photoion coincidence (PEPICO) spectrometer [16].

In Fig. 1, we show the time-dependent parent ion yield from SFI at a fixed polarization geometry of $\alpha' = \alpha'_t = 7°$. The best-fit solid line in Fig. 1 determines the degree of alignment, discussed below. The variation of the CRATI spectra with angle between the alignment and SFI laser polarizations, recorded at the peak alignment $t_a = 58.0$ ps, yields the MF-CAIPs discussed below. The polarization of the SFI pulse was kept parallel to the spectrometer axis, while the alignment laser polarization was systematically varied by a computer controlled achromatic half-wave plate.

In Fig. 2(a), we show the normalized angular ionization yields $M(\alpha', t_a)$ for the parent ion $C_4H_6^+$ D_0 channel (black dots) and the fragment D_1 channels $C_3H_3^+$ (red dots) and $C_4H_5^+$ (green dots) at an intensity of 2.0×10^{13} W/cm^2. The yields show a distinct minimum perpendicular to the alignment axis. In Fig. 3(a), we plot the difference $\Delta M(\alpha')$ between the yield of the parent ion channel and the fragment $C_3H_3^+$ channel from Fig. 2(a), along with the statistical error bars. The angular dependencies of the D_0 and D_1 SFI channels are significantly different. By contrast, the difference in yields between the two fragments $C_3H_3^+$ (red dots) and $C_4H_5^+$ (green dots) is negligible at all α' angles (not shown).

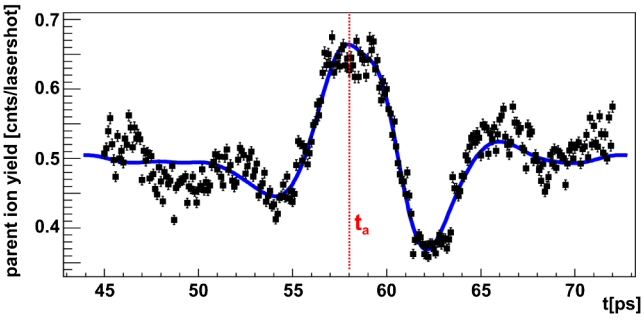

FIG. 1 (color online). Measured time-dependent parent ion yield $M(\alpha'_t, t)$ around the rotational half-revival at a fixed polarization geometry ($\alpha'_t = 7°$). The error bars represent the statistical error based on the number of counts detected. The blue curve represents the best fit, as measured by χ^2.

In order to deconvolve $S(\theta)$ from the measured $M(\alpha', t_a)$ [from Fig. 2(a)], we implemented a self-consistent method that includes a numerical simulation of the molecular alignment. Details of our deconvolution method will be described elsewhere. We simulated time-dependent alignment distributions $A_i(\theta', t)$ using a numerical method developed by Bisgaard and Stapelfeldt [33] for sets $\{T, I\}_i$ of input parameters T (rotational temperature) and I (intensity). As justified in the Supplemental Material [34], we approximated 1,3-butadiene as a symmetric top with rotational constants ($A = 41.1$ GHz, $B = C = 4.2$ GHz) and body-frame polarizabilities ($\alpha_\parallel = 12.2$ Å^3,

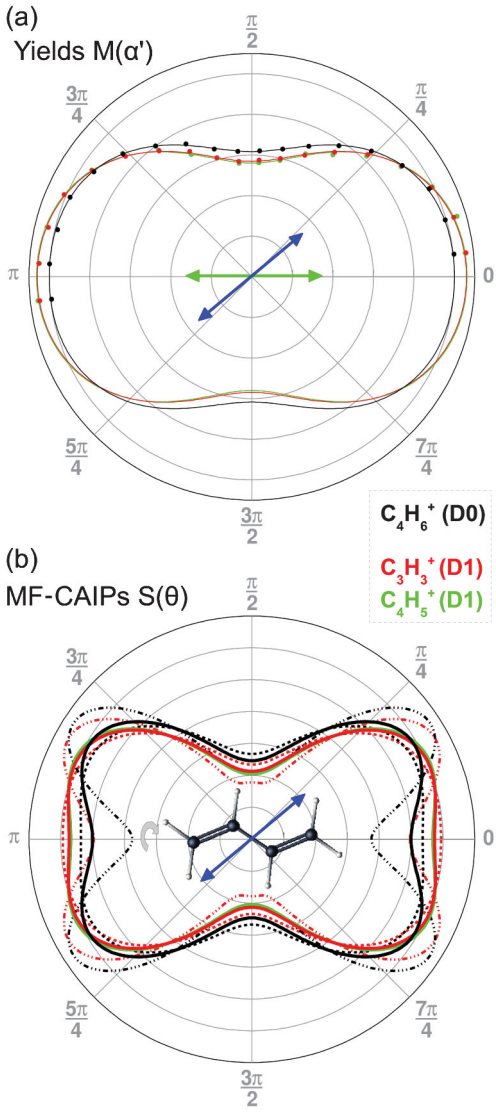

FIG. 2 (color). (a) Lab-frame angular SFI yields $M(\alpha')$ for aligned molecules with fits. Statistical error bars are slightly below the marker size. (b) Deconvolved MF channel-resolved relative angular ionization probabilities $S(\theta)$ (MF-CAIPs) with a 1σ confidence interval. The most polarizable axis of the molecule is aligned horizontally. All distributions are normalized to the same area and displayed on a linear scale.

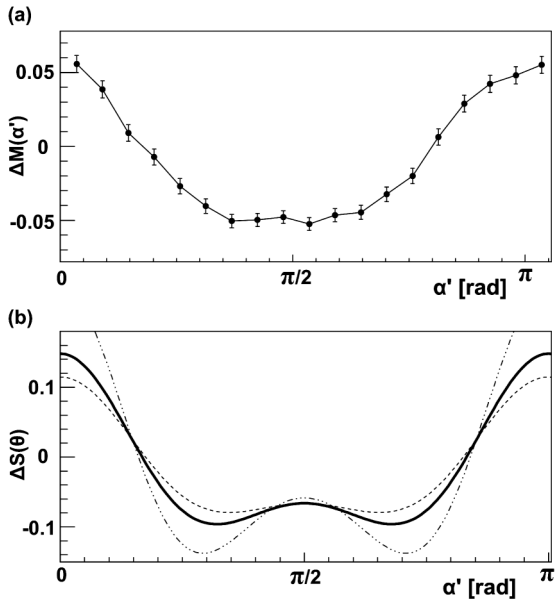

FIG. 3. (a) Difference angular SFI yield $\Delta M(\alpha')$ of the parent ion and the $C_3H_3^+$ fragment of Fig. 2(a) with statistical error bars. (b) Difference $\Delta S(\theta)$ between the MF-CAIPs of the D_0 and D_1 ionization channels in Fig. 2(b) with a 1σ confidence interval (dashed lines).

$\alpha_\perp = 6.2$ Å^3) taken from electronic structure calculations. Reflecting the alignment symmetry, we expressed $S(\theta)$ as a linear combination of even Legendre polynomials

$$S(\theta) = \sum_{k=0}^{k_{\max}} a_{2k} P_{2k}(\cos\theta).$$

Via analysis of fit errors, the appropriate highest order of the expansion was determined to be $k_{\max} = 3$. For each parameter set i, we fit the measured $M(\alpha', t_a)$ data via Eq. (1) using the alignment distribution $A_i(\theta', t_a)$. This generated the deconvolved AIP $S_i(\theta)$ for the ith parameter set. We ranked the deconvolved $S_i(\theta)$ using the measured time-dependent ionization yield $M(\alpha_t', t)$ (from Fig. 1) as a maximum-likelihood predictor. This entailed using $S_i(\theta)$ and $A_i(\theta', t)$ to construct the relative ionization yield time trace $M_i(\alpha_t', t)$ for the ith parameter set via Eq. (1). The χ^2 values of the $M_i(\alpha_t', t)$'s were used to self-consistently identify (i) the MF-CAIP [i.e., the most probable of the AIPs $S_i(\theta)$], (ii) the confidence interval, and (iii) the most probable axis alignment distribution. Note that this analysis gives consistent results for the alignment when applied to both D_0 and D_1 channels.

The solid blue curve in Fig. 1 shows the best-fit $M_i(\alpha_t', t)$, which minimizes the χ^2 value. Good agreement with the measured signal was achieved. The associated parameter set features an alignment laser intensity of $I = 2.375 \times 10^{12}$ W/cm^2 and a rotational temperature of $T = 1.75$ K. The most likely alignment is $\langle\cos^2(\theta_{t_a}')\rangle = 0.69^{+0.06}_{-0.09}$, where the 1σ confidence interval incorporates all alignment distributions for which $\chi^2 \leq \chi^2_{\min} + 1$ [35]. As can be seen, the blue curve shows slightly less modulation than the measured signal, originating from a slight overestimate of spatial averaging or beam temperature or from the symmetric top approximation.

In Fig. 2(b), we show the deconvolved MF-CAIPs, $S(\theta)$, for D_0 and D_1. The absolute confidence intervals are shown as dashed lines. The indistinguishability of the two fragment distributions confirms that they originate from the same SFI channel. The difference between the MF-CAIPs is much more accurately known than the absolute confidence intervals imply. This is because the D_0 and D_1 confidence intervals are not independent but originate from the same underlying best-fit alignment distributions. In Fig. 3(b), we show the difference $\Delta S(\theta)$ between the fragment D_1 and the parent D_0 channels as a solid line, along with its confidence interval (dashed lines). This establishes that the MF-CAIP for ionization to D_1 is clearly distinguished from the MF-CAIP for ionization to D_0. Interestingly, the ionization distributions $S(\theta)$ in Fig. 2(b) do not peak along the most polarizable axis of the molecule (the long axis) but rather at approximately 30° (D_0) and 25° (D_1) with respect to it. The D_0 channel has a more pronounced minimum along the molecular axis, whereas the D_1 channel has a deeper minimum in the perpendicular direction than does the D_0.

We compared our MF-CAIP data with the expectations of both molecular Ammosov-Delone-Krainov (MO-ADK) [11] and time-dependent resolution-in-ionic-states (TD-RIS) [20] calculations. MO-ADK fits the long-range part of the wave function to semiclassical tunnelling functions. These are based on an adiabatic single active electron tunnelling picture that ignores the non-Coulombic effects of the cation potential on the tunneling electron. TD-RIS [20] is a high level time-dependent mixed orbital-grid method, where multielectron orbital-based bound states of the neutral and cationic molecule are coupled to Cartesian grids used to describe the liberated electron. Apart from limitations inherent to the particular choice of basis set and grid size, the present implementation of the method makes only the following assumptions: (i) Only a finite number of cation states are included (we use the lowest seven cation states); (ii) the liberated electron, once removed from the neutral state, is not antisymmetrized with the remaining bound electrons; and (iii) the dipole-mediated laser coupling of the cation states during ionization is excluded. Note that MO-ADK also makes these assumptions in addition to those mentioned above. Details of the underlying electronic structure calculations are described in the Supplemental Material [34]; in particular, diffuse basis functions were used to accurately calculate the tails of the wave functions. In the Hartree-Fock and Koopmans picture, the electron emerges from a specific molecular orbital and the D_0 and D_1 channels become the ionization of highest occupied molecular

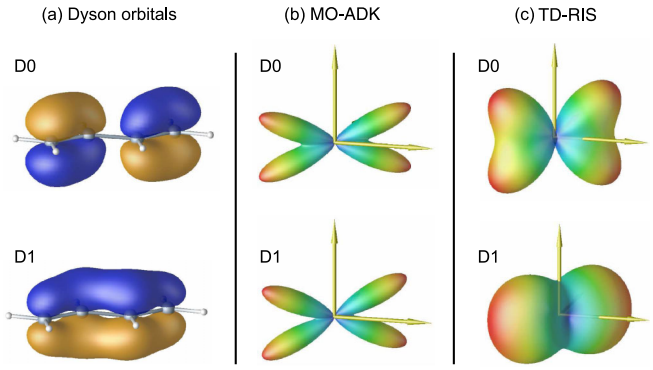

FIG. 4 (color online). (a) Dyson orbitals for ionization of the 1,3-butadiene neutral ground state. Half-cycle 3D ionization probabilities in the MF calculated using (b) MO-ADK and (c) TD-RIS. The MO-ADK distributions for D_0 and D_1 are similar for the reasons outlined in the main text.

orbital (HOMO) and HOMO-1, respectively. At a configuration interaction level of theory, within each ionic channel, the electron originates from a Dyson orbital $|\phi_m^D\rangle = \sqrt{n}\langle I_m|N\rangle$, where $|N\rangle$ is the neutral ground state featuring n electrons and $|I_m\rangle$ is the mth ionic state featuring $n-1$ electrons, with the bra-ket integral taken over the $n-1$ electrons of the ion. The Dyson orbitals—shown in the left column of Fig. 4—were calculated using the procedures outlined in Ref. [36].

While both methods agree that D_0 is the dominant ionization channel at the intensity employed, TD-RIS predicts that the excited cation states should have populations 5% to 15% of that of the D_0 channel (see the Table in the Supplemental Material [34]). In contrast, MO-ADK predicts that the population of the excited cation states is orders of magnitude lower. The experimental data determine that the cumulative yield of all fragments (i.e., including potential sequential dissociation) amounts to 13.0% of the parent ion (D_0) yield. This is the upper limit for direct ionization to excited ion states. The measured yield of the $C_3H_3^+$ and $C_4H_5^+$ fragments is 6.6% of the parent ion yield, which—by virtue of its direct correlation to the lowest cation state—sets the lower limit for D_1 ionization. The experimental D_1 yield is hence in good agreement with the TD-RIS results but incompatible with the MO-ADK results.

The calculated 3D channel-resolved angle-dependent MF ionization yields are shown in the middle (MO-ADK) and right (TD-RIS) columns of Fig. 4. MO-ADK shows a strong suppression of ionization along all nodal planes of the respective Dyson orbitals and also a strong suppression of the D_1 ionization perpendicular to the molecular plane. Within MO-ADK, the latter suppression is a result of the spherical expansion of the long-range wave function. The size of the sphere needed to encompass the long molecular axis yields small wave function amplitudes in perpendicular directions. When these small amplitudes are coupled via MO-ADK to the semiclassical tunneling wave functions, small ionization amplitudes are necessarily produced in the direction perpendicular to the major extent of the molecule. This is likely a general shortcoming of MO-ADK when dealing with extended molecules. The TD-RIS results, however, show that suppression occurs only along the nodal plane perpendicular to the molecular plane, with little or no suppression along the π-like nodal plane that lies within the plane of the molecule.

In order to compare the MF-CAIPs of Fig. 2(b) with theory (Fig. 4), we performed a ϕ average of the latter. This is shown in Fig. 5 for the (a) D_0 and (b) D_1 channels, along with the corresponding experimental data (solid black curves) from Fig. 2(b). The MO-ADK results (dotted blue curves) maximize 20°–25° off the main polarizability axis and show pronounced (D_0) and very pronounced (D_1)

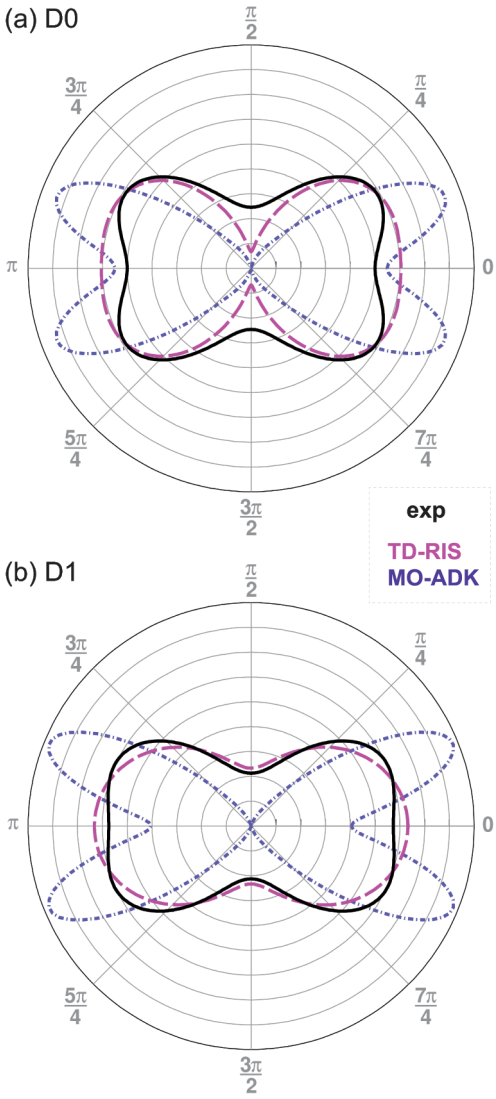

FIG. 5 (color online). Comparison of calculated MO-ADK (dotted blue curves) and TD-RIS (dashed magenta curves) MF-CAIPs with experiment (solid black curves) for (a) D_0 and (b) D_1 ionization.

minima along the major axis. MO-ADK shows very low ionization probability at all angles greater than 45°. In contrast, the TD-RIS results (dashed magenta curves) maximize along the principal axis but retain significant ionization probability in the perpendicular direction. TD-RIS is in much closer overall agreement with experiment for both the D_0 and D_1 channels. MO-ADK systematically overestimates the effect of nodal planes in the Dyson orbitals. In this particular case, TD-RIS slightly underestimates the effect of the nodal planes.

We have extended the CRATI method to the measurement of channel-resolved molecular-frame angular ionization probabilities. The relative contributions of electronic channels to ionization yields depend on molecular alignment, knowledge that is essential for understanding high harmonic generation spectra of molecular systems. We have also shown that MF-CAIPs can be used to critically evaluate different levels of theory. The combination of new experimental measures and new theories of polyatomic SFI will help advance strong-field and attosecond science toward the study of complex polyatomic molecular systems.

We thank C. Z. Bisgaard for stimulating discussions and use of his alignment code and NSERC (Canada) for financial support. J. M. acknowledges support from the Alexander von Humboldt Foundation.

*jochen.mikosch@nrc.ca
†michael.spanner@nrc.ca
‡albert.stolow@nrc.ca

[1] F. Krausz and M. Ivanov, Rev. Mod. Phys. **81**, 163 (2009).
[2] P. Agostini, F. Fabre, G. Mainfray, G. Petite, and N. K. Rahman, Phys. Rev. Lett. **42**, 1127 (1979).
[3] P. B. Corkum, Phys. Rev. Lett. **71**, 1994 (1993).
[4] M. Spanner, O. Smirnova, P. B. Corkum, and M. Y. Ivanov, J. Phys. B **37**, L243 (2004).
[5] M. Meckel *et al.*, Science **320**, 1478 (2008).
[6] L. V. Keldysh, Zh. Eksp. Teor. Fiz. **47**, 1945 (1964) [Sov. Phys. JETP **20**, 1307 (1965)].
[7] A. M. Perelomov, V. S. Popov, and M. V. Terent'ev, Zh. Eksp. Teor. Fiz. **50**, 1393 (1966) [Sov. Phys. JETP **23**, 924 (1966)]; A. M. Perelomov, V. S. Popov, and M. V. Terent'ev, Zh. Eksp. Teor. Fiz. **51**, 309 (1966) [Sov. Phys. JETP **24**, 207 (1967)].
[8] M. V. Ammosov, N. B. Delone, and V. P. Krainov, Zh. Eksp. Teor. Fiz. **91**, 2008 (1986) [Sov. Phys. JETP **64**, 1191 (1986)].
[9] M. Lezius, V. Blanchet, D. M. Rayner, D. M. Villeneuve, A. Stolow, and M. Y. Ivanov, Phys. Rev. Lett. **86**, 51 (2001).
[10] M. Smits, C. A. de Lange, A. Stolow, and D. M. Rayner, Phys. Rev. Lett. **93**, 203402 (2004).
[11] X. M. Tong, Z. X. Zhao, and C. D. Lin, Phys. Rev. A **66**, 033402 (2002).
[12] J. Muth-Böhm, A. Becker, and F. H. M. Faisal, Phys. Rev. Lett. **85**, 2280 (2000).
[13] O. Smirnova, Y. Mairesse, S. Patchkovskii, N. Dudovich, D. Villeneuve, P. Corkum, and M. Y. Ivanov, Nature (London) **460**, 972 (2009).
[14] B. K. McFarland, J. P. Farrell, P. H. Bucksbaum, and M. Guhr, Science **322**, 1232 (2008).
[15] H. Akagi, T. Otobe, A. Staudte, A. Shiner, F. Turner, R. Dorner, D. M. Villeneuve, and P. B. Corkum, Science **325**, 1364 (2009).
[16] A. E. Boguslavskiy, J. Mikosch, A. Gijsbertsen, M. Spanner, S. Patchkovskii, N. Gador, M. J. J. Vrakking, and A. Stolow, Science **335**, 1336 (2012).
[17] X. Chu and S.-I. Chu, Phys. Rev. A **70**, 061402 (2004).
[18] D. Dundas and J. M. Rost, Phys. Rev. A **71**, 013421 (2005).
[19] T. Otobe and K. Yabana, Phys. Rev. A **75**, 062507 (2007).
[20] M. Spanner and S. Patchkovskii, Phys. Rev. A **80**, 063411 (2009); Chem. Phys. (to be published).
[21] A. S. Alnaser, S. Voss, X. M. Tong, C. M. Maharjan, P. Ranitovic, B. Ulrich, T. Osipov, B. Shan, Z. Chang, and C. L. Cocke, Phys. Rev. Lett. **93**, 113003 (2004).
[22] D. Pavicic, K. F. Lee, D. M. Rayner, P. B. Corkum, and D. M. Villeneuve, Phys. Rev. Lett. **98**, 243001 (2007).
[23] L. Holmegaard *et al.*, Nat. Phys. **6**, 428 (2010).
[24] S.-F. Zhao, J. Xu, C. Jin, A.-T. Le, and C. D. Lin, J. Phys. B **44**, 035601 (2011).
[25] A. Fleischer, H. J. Worner, L. Arissian, L. R. Liu, M. Meckel, A. Rippert, R. Dorner, D. M. Villeneuve, P. B. Corkum, and A. Staudte, Phys. Rev. Lett. **107**, 113003 (2011).
[26] Z. B. Walters and O. Smirnova, J. Phys. B **43**, 161002 (2010).
[27] M. Abu-Samha and L. B. Madsen, Phys. Rev. A **82**, 043413 (2010).
[28] A. S. Alnaser, C. M. Maharjan, X. M. Tong, B. Ulrich, P. Ranitovic, B. Shan, Z. Chang, C. D. Lin, C. L. Cocke, and I. V. Litvinyuk, Phys. Rev. A **71**, 031403 (2005).
[29] H. Stapelfeldt and T. Seideman, Rev. Mod. Phys. **75**, 543 (2003).
[30] J. L. Hansen, L. Holmegaard, J. H Nielsen, H. Stapelfeldt, D. Dimitrovski, and L. B. Madsen, J. Phys. B **45**, 015101 (2012).
[31] J. L. Hansen *et al.*, Phys. Rev. A **83**, 023406 (2011).
[32] D. Dimitrovski, M. Abu-samha, L. B. Madsen, F. Filsinger, G. Meijer, J. Kupper, L. Holmegaard, L. Kalhoj, J. H. Nielsen, and H. Stapelfeldt, Phys. Rev. A **83**, 023405 (2011).
[33] C. Z. Bisgaard, Ph.D. Thesis, University of Aarhus, 2006.
[34] See Supplemental Material at http://link.aps.org/supplemental/10.1103/PhysRevLett.110.023004 for additional details regarding both the experimental procedures and the theoretical methods.
[35] P. J. Cumpson and M. P. Seah, Surf. Interface Anal. **18**, 345 (1992).
[36] S. Patchkovskii, Z. Zhao, T. Brabec, and D. M. Villeneuve, J. Chem. Phys. **126**, 114306 (2007).